Inorganic Chemistry
Article
pubs.acs.org/IC

Formation Mechanism of (001) Oriented Perovskite $SrTiO_3$ Microplatelets Synthesized by Topochemical Microcrystal Conversion

Yunfei Chang,*[†] Huanpo Ning,[‡] Jie Wu,[†] Shantao Zhang,[§] Tianquan Lü,[†] Bin Yang,*[†] and Wenwu Cao[†,∥]

[†]Condensed Matter Science and Technology Institute & School of Science, Harbin Institute of Technology, Harbin 150080, China
[‡]School of Engineering and Materials Science, Queen Mary University of London, London E1 4NS, U.K.
[§]National Laboratory of Solid State Microstructures & Department of Materials Science and Engineering, Nanjing University, Nanjing 210093, China
[∥]Department of Mathematics and Materials Research Institute, The Pennsylvania State University, University Park, Pennsylvania 16802, United States

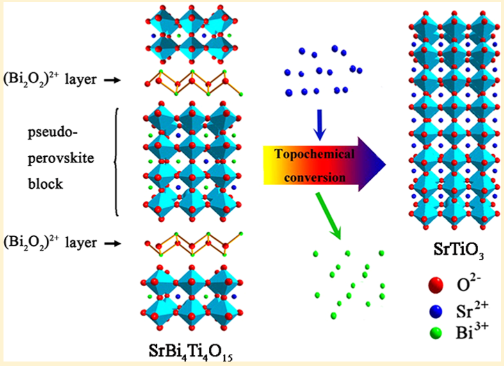

ABSTRACT: To develop a better understanding of the mechanism responsible for topochemical microcrystal conversion (TMC) from Aurivillius $SrBi_4Ti_4O_{15}$ precursors to perovskite $SrTiO_3$ microplatelets, compositional/structural evolutions, morphological development, and reaction interface evolution of the (001) oriented $SrBi_4Ti_4O_{15}$ microplatelets were investigated during the conversion process. The results show that multiple topotactic nucleation events of $SrTiO_3$ occurred directly on the surfaces of $SrBi_4Ti_4O_{15}$ above 700 °C, while reacting zones of intermediate phase(s) with less Bi^{3+} contents were observed to form in the interior of $SrBi_4Ti_4O_{15}$. Extensive exfoliation of the precursors occurred generally parallel to the (001) surfaces above 775 °C. At 950 °C, the original single-crystal $SrBi_4Ti_4O_{15}$ platelet was replaced by a polycrystalline aggregate consisting of (001) aligned $SrTiO_3$ crystallites and poorly crystallized intermediate phase(s). With further increasing the temperature or holding time, the $SrTiO_3$ phase formed from related intermediate phase(s), and the aligned crystallites were sintered to form dense $SrTiO_3$ with strong (001) orientation. The obtained $SrTiO_3$ microplatelets preserved the shape of $SrBi_4Ti_4O_{15}$ and show high chemical and phase purity. This TMC mechanism has general applicability to a variety of compounds and will be very useful for the design and synthesis of novel anisotropic perovskite crystals with high quality in the future.

1. INTRODUCTION

Anisotropic perovskites (ABO_3) have recently attracted intensive attention because of their favorable shape-dependent properties and their wide applications in thin films, highly textured ceramics via (reactive) templated grain growth (TGG), and single crystals by seeded polycrystal conversion, where they serve as ideal substrates or templates to seed oriented grain growth for achieving optimum electrical properties of various materials.[1−3] Anisotropic perovskite crystals, however, are difficult to synthesize via a conventional solid-state reaction method due to the high symmetry of crystal structure. Soft chemistry offers the potential for controlling thermodynamically inaccessible structural and morphological features at the kinetic level.[4] As one kind of soft chemistry method, topochemical microcrystal conversion (TMC) associated with the use of localized solid-state compound transformations through exchange, deflection, or insertion of individual atom offers one of the most effective strategies to the conscious manipulation of material synthesis with desired structures.[4−6] Several perovskite compounds with highly anisotropic morphologies and/or controlled orientations, such as $KNbO_3$ needles, (Na, K)NbO_3 nanobars, and $NaNbO_3$, $BaTiO_3$, (Ba,Ca)TiO_3, and $PbTiO_3$ based platelets, have been produced by conversion of structurally related precursors via a topotactic or epitaxial growth process.[7−11]

Strontium titanate ($SrTiO_3$) is a unique intriguing multifunctional perovskite structural compound with a simple cubic crystal structure. It exhibits different properties, such as ferroelectricity, microwave dielectric tenability, high electronic conductivity, quantum paraelectricity, oxygen conductivity, and photocatalytic behavior, depending on the oxygen stoichiometry, doping, and strain state.[12−17] In recent years, a number of chemical synthesis techniques have been developed to fabricate $SrTiO_3$ crystals, such as hydrothermal synthesis, sol−gel method, coprecipitation, microemulsion, etc.[17−20]Among them, topochemical synthesis of anisometric $SrTiO_3$ microcrystals attracts special attention, especially considering the

Received: July 5, 2014
Published: October 6, 2014

dx.doi.org/10.1021/ic501604c | *Inorg. Chem.* 2014, 53, 11060−11067

widespread use of $SrTiO_3$ platelets for production of grain oriented perovskite films/textured ceramics/single crystals due to both similar structures and chemical stability at high temperatures. Watari et al.[21] was the first to report that Ruddlesden−Popper-type layered perovskite $Sr_3Ti_2O_7$ (a = 0.390 nm and c = 2.038 nm) can be converted into (001) oriented and anisotropically shaped $SrTiO_3$ platelets (a = 0.390 nm) under TMC conditions. Subsequently, Liu,[22] Ebrahimi,[23] and Akdogan[24] et al. investigated, respectively, the effects of starting TiO_2 powders (rutile or anatase) and processing parameters (such as flux amount and type, temperature, etc.) on morphology and size of $Sr_3Ti_2O_7$ and $SrTiO_3$ particles in order to achieve a high aspect ratio of $SrTiO_3$ platelets. In the reaction of Ruddlesden−Popper $Sr_3Ti_2O_7$ to perovskite $SrTiO_3$, the nucleation and epitaxial growth of $SrTiO_3$ from the (001) surfaces of the $Sr_3Ti_2O_7$ precursor phase occurs due to the similar atomic configurations of the {001} planes of Ruddlesden−Popper and perovskite structures.[25] However, this complete conversion requires a high reaction temperature of above 1200 °C, and the obtained $SrTiO_3$ particles have a large size of about 20−50 μm × 2−4 μm, which inhibited their sinterability.[26] In addition, employment of such big template particles resulted in coarsened microstructure and compromised the mechanical strength of textured ceramics.[27] Recently, Saito et al.[26] developed a novel strategy to produce (001) oriented $SrTiO_3$ platelets with a smaller particle size of about 5−10 μm × 0.5 μm by converting Aurivillius phase $SrBi_4Ti_4O_{15}$ at a significantly reduced temperature of ∼950 °C, but Bi^{3+} was not effectively removed from the converted products (Bi^{3+} remained 10.3 at % in the A-site positions of the perovskite structure). Subsequently, these small $SrTiO_3$ platelets have been, respectively, used as templates to seed oriented grain growth in $SrTiO_3$, (Ba, Sr)TiO_3, (Bi, Na)TiO_3-$SrTiO_3$, $Bi_{0.5}(Na, K)_{0.5}TiO_3$, and $(Bi_{0.95}Na_{0.75}K_{0.15}Li_{0.05})_{0.5}Ba_{0.05}TiO_3$ based textured ceramics/films, etc.[28−31] The existence of residual Bi^{3+} in the templates tends to bring impurity ions into ceramics/films, which may result in the formation of some defects (e.g., A-site and/or B-site vacancies)[32] and/or secondary phases segregated at the grain boundaries,[33] leading to inhibition of grain growth and preventing the evolution of grain orientation.[34] Hence, excess Bi^{3+} ions would deteriorate the densification behavior, the formation of texture, and/or electrical properties of some textured ceramics/films.[35] Therefore, particular attention should be paid to the TMC process, which determines the final quality of converted products. In order to synthesize high-quality $SrTiO_3$ microplatelets, it is crucial to study the mechanism responsible for topochemical and morphological conversion from Aurivillius $SrBi_4Ti_4O_{15}$ to perovskite $SrTiO_3$. In addition, the understanding and control of the mechanism would be beneficial for the design and synthesis of advanced structural and functional materials in the future. Although the TMC method has been used by Saito et al.[26] to fabricate anisotropic $SrTiO_3$, the conversion mechanism of the Aurivillius $SrBi_4Ti_4O_{15}$ to perovskite $SrTiO_3$ has not been identified. For $SrBi_4Ti_4O_{15}$ precursors, the Aurivillius structure consists of insulating $(Bi_2O_2)^{2+}$ layers and pseudo-perovskite $(A_{n-1}B_nO_{3n+1})^{2-}$ blocks stacked along the c axis, where A represents the mixture of Sr^{2+} and Bi^{3+}, B represents Ti^{4+}, and n = 4 is the layer number of BO_6 octahedrons in $SrBi_4Ti_4O_{15}$ (Figure 1). Compared with the conversion of $SrTiO_3$ from Ruddlesden−Popper-type $Sr_3Ti_2O_7$, the Aurivillius $SrBi_4Ti_4O_{15}$ to perovskite $SrTiO_3$ reaction is more complicated because of the need to remove Bi^{3+} from the precursor phase.

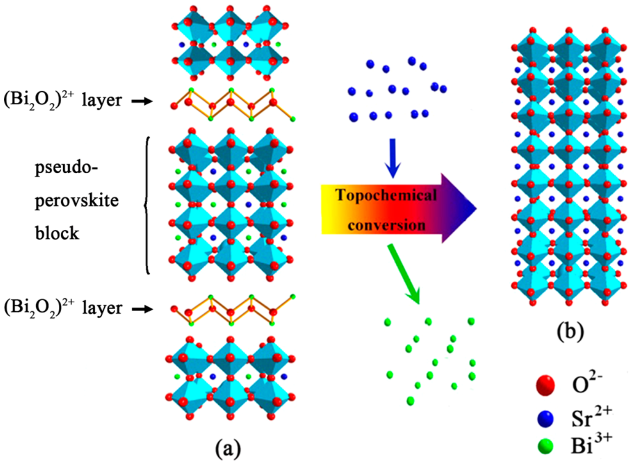

Figure 1. Schematic illustration of crystal structure and conversion scheme of TMC reaction: (a) Aurivillius $SrBi_4Ti_4O_{15}$; (b) perovskite $SrTiO_3$.

In this work, (001) oriented $SrTiO_3$ microplatelets with controlled morphologies and high aspect ratios were fabricated by topochemical microcrystal conversion (TMC) in KCl salt. The objective of this study is to develop a better understanding of the TMC mechanism in perovskite $SrTiO_3$ based on Aurivillius $SrBi_4Ti_4O_{15}$ precursors, which differs substantially from that based on Ruddlesden−Popper-type layered perovskite $Sr_3Ti_2O_7$ precursors. Compositional/structural evolution, morphological development, and reaction interface evolution during the Aurivillius $SrBi_4Ti_4O_{15}$ to perovskite $SrTiO_3$ conversion were investigated by X-ray diffraction, Raman scattering, differential thermal analysis, field-emission scanning electron microscopy, transmission electron microscopy measurements, etc.

2. EXPERIMENTAL PROCEDURE

Aurivillius $SrBi_4Ti_4O_{15}$ precursors were produced by molten salt synthesis (MSS).[36] Stoichiometric amounts of $SrCO_3$, Bi_2O_3, and TiO_2 were mixed according to eq 1 by ball-milling in ethanol for 12 h. In order to get high-aspect-ratio $SrBi_4Ti_4O_{15}$ microplatelets with a relatively narrow size distribution, an equal weight of KCl salt was added, and the raw materials were mixed again for 12 h. The dried powder mixture was put into a sealed alumina crucible and heated at 1115 °C for 6 h. The flux was removed from the products by repeated washing with hot deionized water.

$$SrCO_3 + 2Bi_2O_3 + 4TiO_2 \rightarrow SrBi_4Ti_4O_{15} + CO_2 \qquad (1)$$

$$SrBi_4Ti_4O_{15} + 3SrCO_3 \rightarrow 4SrTiO_3 + 2Bi_2O_3 + 3CO_2 \qquad (2)$$

Perovskite $SrTiO_3$ platelets were obtained by topochemical microcrystal conversion (TMC) based on $SrBi_4Ti_4O_{15}$ precursors according to eq 2. Because a little higher $SrCO_3$ content would facilitate the chemical conversion from $SrBi_4Ti_4O_{15}$ to $SrTiO_3$ and be more favorable for perovksite phase formation, $SrBi_4Ti_4O_{15}$ precursors were reacted with $SrCO_3$ powder in a molar ratio of 1:4.5. An equal weight of KCl was added as flux. $SrCO_3$ was first mixed with KCl by ball-milling in ethanol for 12 h, and then $SrBi_4Ti_4O_{15}$ precursors were added by magnetic stirring to avoid destroying the platelike shape of $SrBi_4Ti_4O_{15}$. The dried powder mixtures were heated at 4 °C/min to between 600 and 1050 °C and immediately air quenched to observe the structural evolution and morphological development of the $SrBi_4Ti_4O_{15}$ precursors. Afterward, large batches of $SrTiO_3$ microplatelets were synthesized at 950 °C for 3 h. The flux was removed by washing with deionized water repeatedly, after which the byproduct

Bi_2O_3 was removed by soaking in 30% HNO_3 for 1−3 h. Finally, the product was rinsed using deionized water for a few times again.

The phase purity and crystal structure were determined by X-ray diffraction (XRD, D/max 2400, Rigaku Corporation, Tokyo, Japan). For phase evolution analysis, quenched samples prepared as described above were gently soaked in deionized water to remove flux and then were ground to minimize the preferred orientation. Front loading sample holders (zero background silicon) were used with a fixed area geometry.[9,37] Phases in each sample were identified using the software package MDI Jade 9 (Materials Data Inc., Livermore, CA, USA). The total peak intensity for each phase of interest was calculated by profile fitting of the relevant peaks in each data set and adding their intensities together, after subtracting the background. Peak intensities between 10° and 70° (2θ) were used for this calculation. Raman scattering investigation was performed at room temperature by using a LabRAM XploRA spectrometer (HORIBA Jobin Yvon S.A.S., France). Morphological and compositional characterizations were performed using field-emission scanning electron microscopy (FE-SEM, HELIOS NanoLab 600i, FEI Corporation, OR, USA) in combination with energy-dispersive X-ray spectrometry (EDS). For the morphological evolution study, quenched samples were gently soaked in deionized water to remove flux, and no other powder preparation (such as grinding, soaking in HNO_3, etc.) was used so as to avoid significantly damaging the fine morphology features on the platelike particle surfaces. To determine the transformations during the heating process, differential thermal analysis (DTA) and thermogravimetric analysis (TG) of the powder mixtures were performed using Thermoanalyzer Systems (Q600SDT, TA Instruments, USA). To investigate morphology/chemical composition evolutions in the interior of the samples, the cross sections of platelets were obtained via focused ion beam (FIB, HELIOS NanoLab 600i) and observed by using a field-emission gun transmission electron microscope (FEG-TEM, Tecnai G2 F30, FEI Corporation, OR, USA) in combination with energy-dispersive X-ray spectrometry (EDS). The specimens for FIB thinning were dispersed on single-crystal Si substrates and coated with Pt to prevent charging, and those platelets lying flat were selected and transferred to TEM grids via manipulator. Cross sections of samples were obtained by cutting parallel to the platelet normal, close to an expected [001] perovskite zone axis. Thinning was performed at 80 pA with the final cleaning at 40 pA.

3. RESULTS AND DISCUSSION

Figure 1 shows the schematic illustration of the crystal structure conversion from Aurivillius phase $SrBi_4Ti_4O_{15}$ to perovskite phase $SrTiO_3$. During the conversion process, the $(Bi_2O_2)^{2+}$ slabs in $SrBi_4Ti_4O_{15}$ will be removed during heat treatment. Sr^{2+} will diffuse into pseudo-perovskite $(A_{n-1}B_nO_{3n+1})^{2-}$ blocks and replace Bi^{3+} ions in the A-site through topochemical techniques and form a $SrTiO_3$ perovskite phase.

The XRD patterns of $SrBi_4Ti_4O_{15}$ precursors and $SrTiO_3$ microcrystals converted at 950 °C for 3 h and cast on glass substrates are shown in Figure 2a, respectively. From the XRD patterns, it can be seen that $SrBi_4Ti_4O_{15}$ particles are of pure Aurivillius phase, corresponding to an orthorhombic structure (PDF # 43-0973, a = 0.543 nm, b = 0.544 nm, and c = 4.094 nm).[38] The strong intensities of (00l) diffraction peaks indicate that these $SrBi_4Ti_4O_{15}$ microcrystals have a strong anisotropic growth in these planes. In addition, the converted microcrystals are identified to be of single-phase perovskite $SrTiO_3$ with a cubic structure (PDF # 74-1296, a = 0.390 nm)[39] and have a strong (00l) orientation, which is different from the random orientation of $SrTiO_3$ particles prepared by the conventional method.[19] This indicates that the {001} plane of $SrBi_4Ti_4O_{15}$ is converted into the {001} plane of $SrTiO_3$ during topochemical reaction.

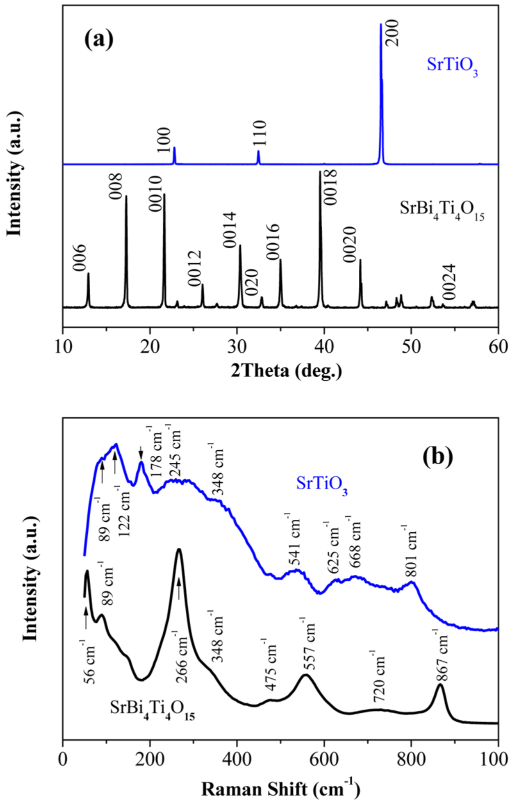

Figure 2. (a) XRD patterns and (b) Raman spectra of Aurivillius $SrBi_4Ti_4O_{15}$ precursors and perovskite $SrTiO_3$ microcrystals converted at 950 °C for 3 h.

Raman scattering is known to be an appropriate technique for the investigation of the short-range order, phase structure, and space group in advanced materials. Figure 2b shows the Raman responses of $SrBi_4Ti_4O_{15}$ precursors and converted $SrTiO_3$ microcrystals. It can be seen that the Raman spectrum of Aurivillius $SrBi_4Ti_4O_{15}$ precursors exhibits intense phonon modes at around 56, 89, 266, 557, and 867 cm^{-1} and some weak peaks, which is similar to that of $SrBi_4Ti_4O_{15}$ prepared by the conventional method reported by Kojima et al.[40,41] The sharp mode at around 56 cm^{-1} is due to the displacement of Bi^{3+} ions in $(Bi_2O_2)^{2+}$ slabs, and that at about 89 cm^{-1} is related to the vibration of Bi^{3+} and Sr^{2+} ions in the A-sites of the pseudo-perovskite blocks.[40] The mode at the ∼266 cm^{-1} band is the internal angle bending vibration, while those observed at ∼557 and 867 cm^{-1} relate to the stretching vibrations of TiO_6 octahedra.[40,41] Here, the modes above 200 cm^{-1} are classified as internal modes of the TiO_6 octahedra. For converted perovskite $SrTiO_3$ particles, the Raman response is different from that of $SrBi_4Ti_4O_{15}$ precursors because of the different phase structures. At room temperature, $SrTiO_3$ has an ideal cubic perovskite structure, and the room-temperature spectrum should be dominated by second-order scattering on the basis of factor group symmetry analysis.[42] A low-frequency band at 89 cm^{-1} and two second-order broad bands centered in the 200−400 and 600−800 cm^{-1} regions can be observed from Figure 2b, which are similar to that of equiaxed $SrTiO_3$ prepared by the conventional method.[19,43] Moreover, the Raman spectrum of converted $SrTiO_3$ particles displays several interesting features beyond second-order bands. Specifically, it shows four additional peaks at 122, 178, 541, and 801 cm^{-1}, which cannot be detected from that of $SrTiO_3$ prepared by conventional the method. Rabuffetti et al.[19] reported the existence of those peaks in the Raman spectra of $SrTiO_3$

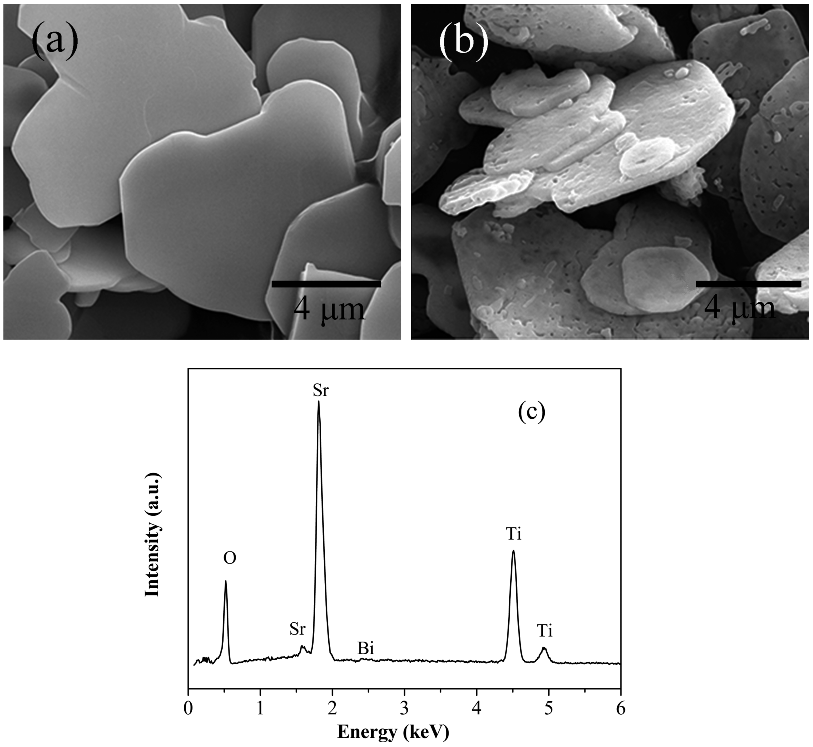

Figure 3. (a) SEM image of Aurivillius $SrBi_4Ti_4O_{15}$ precursors, and (b) SEM image and (c) EDS profile of perovskite $SrTiO_3$ microcrystals converted at 950 °C for 3 h.

nanocubes fabricated by MSS and sol-precipitation coupled with hydrothermal synthesis, and they suggested that those peaks may arise from first-order Raman activity.

SEM micrographs of (a) Aurivillius $SrBi_4Ti_4O_{15}$ precursors and (b) perovskite $SrTiO_3$ microcrystals converted at 950 °C for 3 h are shown in Figure 3. $SrBi_4Ti_4O_{15}$ precursors show a platelike morphology with an average length of ~5 μm and an average thickness of ~0.4 μm. During the TMC reaction, the morphology of single-crystalline $SrBi_4Ti_4O_{15}$ precursors was preserved. The derived $SrTiO_3$ particles also show a platelike shape with about 5 μm in average length and around 0.4 μm in average thickness. Most particles are observed to be polycrystalline, although some smaller ones are devoid of grain boundaries. These grain boundaries are residual from the TMC process. To evaluate the atomic composition of the resultant microcrystals, the EDS profile was measured and is displayed in Figure 3c. It shows a pattern like that of pure $SrTiO_3$. Sr^{2+} occupies about 99.1 at % in A-site positions, and a tiny amount of Bi^{3+} (~0.9 at %) was detected, which is much lower than that (~10.3 at %) reported by Saito et al.[26] In this work, $SrTiO_3$ microcrystals were fabricated via a tailored topochemical conversion process at optimized processing conditions, including the suitable molar ratio (1:4.5) of $SrBi_4Ti_4O_{15}/SrCO_3$, optimum heating rate (4 °C/min)/reaction temperature (950 °C)/reaction time (3 h), and careful control of washing procedures. All of these are very beneficial to more complete substitution of Sr^{2+} for Bi^{3+} in $SrBi_4Ti_4O_{15}$ precursors and effective removal of residual Bi^{3+} from final products. The $SrTiO_3$ platelets are nearly the ideal substrate or template candidate to seed oriented grain growth for achieving optimum electrical properties of various materials.

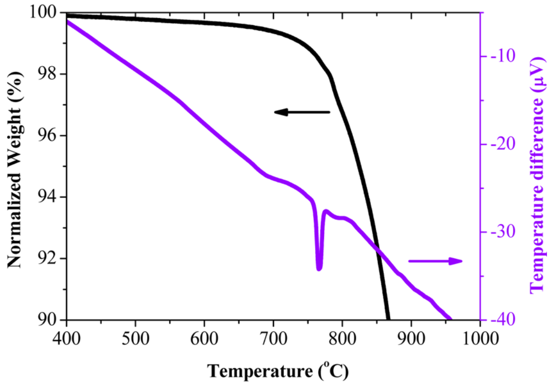

Figure 4. TG and DTA characterizations of the Aurivillius $SrBi_4Ti_4O_{15}$ to perovskite $SrTiO_3$ conversion process.

Figure 4 shows TG and DTA characterizations of the Aurivillius $SrBi_4Ti_4O_{15}$ to perovskite $SrTiO_3$ conversion process. A strong endothermic peak is observed at around 770 °C due to the melting of KCl salt. An obvious weight loss occurs from ~700 °C due to the onset of decomposition of $SrCO_3$. Because pure $SrCO_3$ did not show significant weight loss below 1000 °C, the decomposition of $SrCO_3$ is caused by the direct reaction of the carbonate with $SrBi_4Ti_4O_{15}$ precursors. Before the melting point of KCl at ~770 °C, a weight loss of ~1.5% can be observed, which is less than the theoretical loss of 3.3% caused by CO_2 removal for the complete conversion process (eq 2). This means that the reaction between $SrCO_3$ and $SrBi_4Ti_4O_{15}$ happens in a broad temperature range. Continuous decomposition of $SrCO_3$ and the evaporation of flux resulted in further weight loss by increasing the temperature above 770 °C. Because of the long process of Aurivillius to perovskite conversion and CO_2 removal, weak signals associated with these were masked and cannot be clearly observed in the DTA curve. This also indicates that the topochemical reaction is not strongly endothermic or exothermic.

Phase evolution during the Aurivillius $SrBi_4Ti_4O_{15}$ to perovskite $SrTiO_3$ conversion process is shown as a function of heat treatment in Figure 5. Samples initially consist of $SrBi_4Ti_4O_{15}$ and $SrCO_3$ phases, and they do not react until 700 °C. Perovskite $SrTiO_3$ begins to form at 750 °C, and its intensity increases with further increasing the temperature. An intermediate layer structure(s) is (are) detected, but the identity of these phases could not be confirmed due to very broad peaks (Figure 5b) as a result of low crystallinity. The $SrBi_4Ti_4O_{15}$ phase completely converts into the intermediate layer structured phase(s) and $SrTiO_3$ at 900 °C, and the total peak intensity of these intermediate phases maximizes at around 900−950 °C. Perovskite $SrTiO_3$ formation accelerates rapidly above 950 °C, at which point intermediate phases are rapidly consumed. In addition, $SrCO_3$ gradually disappears during the heating treatment and appears to be coincident with $SrTiO_3$ phase formation. Finally, Aurivillius $SrBi_4Ti_4O_{15}$ to perovskite $SrTiO_3$ conversion completes at 1050 °C with perovskite $SrTiO_3$ and byproduct Bi_2O_3 detected in the samples.

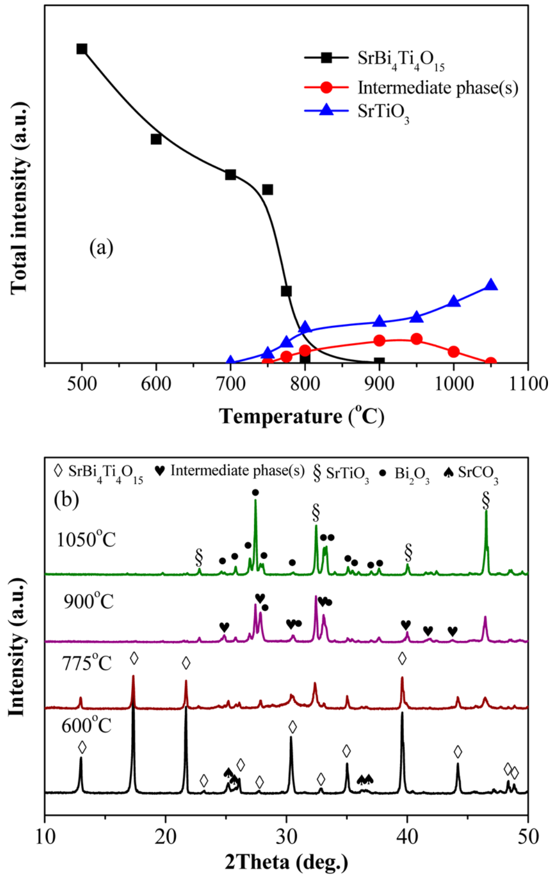

Figure 5. (a) Sequence of phase formation during the Aurivillius $SrBi_4Ti_4O_{15}$ to perovskite $SrTiO_3$ conversion process as measured by the total XRD peak intensity, and (b) selected XRD patterns, showing $SrBi_4Ti_4O_{15}$, $SrCO_3$, intermediate phase(s), and $SrTiO_3$, respectively.

Figure 6 shows morphology evolution of the particles during the topochemical conversion process from Aurivillius $SrBi_4Ti_4O_{15}$ to perovskite $SrTiO_3$. The $SrBi_4Ti_4O_{15}$ precursors show a relatively smooth surface at 600 °C. According to Figures 4 and 5, $SrBi_4Ti_4O_{15}$ and $SrCO_3$ began to react in the solid state prior to melting of KCl at 770 °C. From Figure 6, it can be seen that $SrBi_4Ti_4O_{15}$ platelets act as insoluble sites for the nucleation and growth of $SrTiO_3$. Both the surface and the lateral face of $SrBi_4Ti_4O_{15}$ platelets become rough, and many distinct nanocrystallites are visible at 750 °C, indicating the multiple topotactic nucleation events of $SrTiO_3$ directly on the $SrBi_4Ti_4O_{15}$ precursor surfaces and lateral faces. In addition, many cracks nearly parallel to the surfaces can be seen from the lateral faces. Extensive exfoliation of the platelike crystals occurs generally parallel to the surfaces at 800 °C, and many nano "grains" and some nanosized pores among "grains" can be observed in layers of each microcrystal. The topochemical reaction accelerates after KCl melting at ~770 °C. That may be because of the enhanced diffusion of Sr^{2+} and O^{2-} in the vicinity of layers inside and at the surfaces of precursor platelets due to the finite solubility of SrO in KCl flux. With increasing the temperature to 950 °C, perovskite $SrTiO_3$ nanocrystallites grow into larger sizes and the original $SrBi_4Ti_4O_{15}$ platelet is replaced by a polycrystalline aggregate consisting of aligned perovskite grains and poorly crystalline intermediate phase(s). With further increasing the temperature or holding time, intermediate phase(s) is (are) consumed and the polycrystalline aggregates recrystallize and sinter to form dense perovksite $SrTiO_3$ platelets with (001) orientation (Figure 3b).

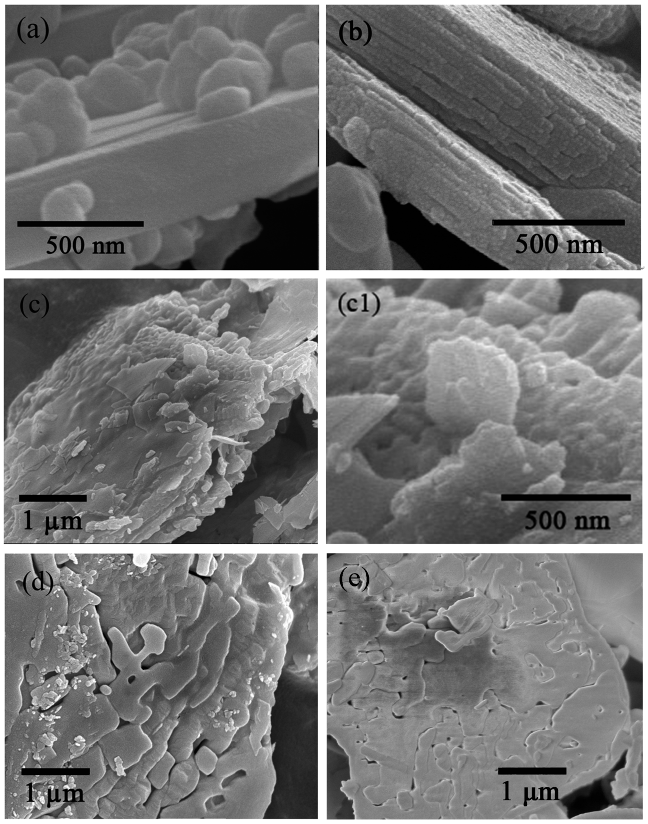

Figure 6. Morphology evolution during the Aurivillius $SrBi_4Ti_4O_{15}$ to perovskite $SrTiO_3$ conversion process. Samples were, respectively, heated to (a) 600, (b) 750, (c, c1) 800, (d) 900, and (e) 950 °C and were immediately air quenched.

According to the results of Figures 5 and 6, the $SrBi_4Ti_4O_{15}$ microcrystals heated at 775 °C were selected as the specimens for TEM observation to better investigate the TMC path of perovskite $SrTiO_3$ based on Aurivillius $SrBi_4Ti_4O_{15}$. Bright-field TEM images of the cross section of a $SrBi_4Ti_4O_{15}$ platelet and a

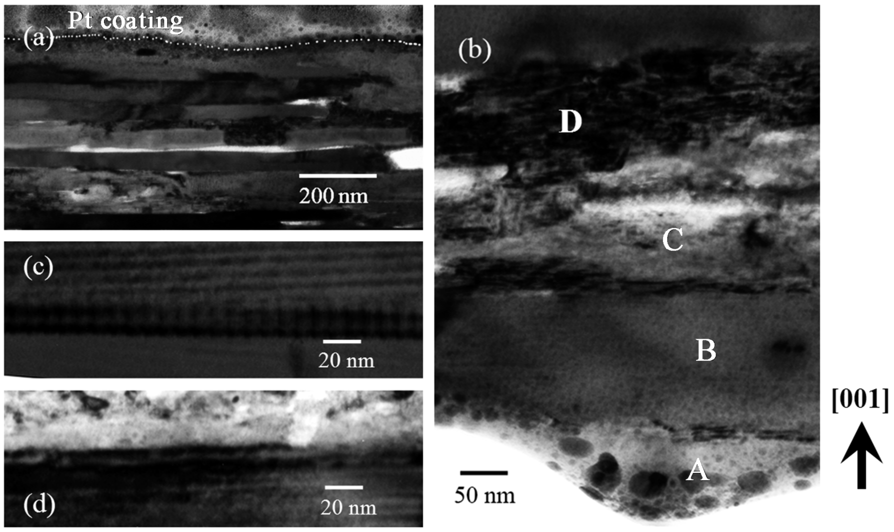

Figure 7. (a) Bright-field TEM image of cross section of an Aurivillius $SrBi_4Ti_4O_{15}$ platelet during topochemical conversion into perovskite $SrTiO_3$ at 775 °C, (b) a closer image showing a region containing (A) surface $SrTiO_3$ zones, (B) $SrBi_4Ti_4O_{15}$ zones inside, and (C and D) reacting zones inside, and images showing misalignment and/or defects near the interface between (c) the reacting zone and the $SrBi_4Ti_4O_{15}$ zone or (d) reacting zones.

selected region are shown in Figure 7a,b, respectively. In addition, Table 1 shows the atomic compositions of A, B, C, and D regions marked in Figure 7b. According to Figure 5, the platelets heated to 775 °C consist of $SrBi_4Ti_4O_{15}$ and $SrTiO_3$ phases, as well as intermediate layer structure phase(s). It can be seen from Figure 7 that the platelet surfaces are covered with $SrTiO_3$ zones that contained numerous poorly crystalline $SrTiO_3$ grains (i.e., A region in Figure 7b). Many pores of various sizes can be seen in this zone. Both raw $SrBi_4Ti_4O_{15}$ zones (i.e., B region in Figure 7b) and reacting zones containing intermediate phase(s) (i.e., C and D regions in Figure 7b) can be observed inside the platelet after reaction at 775 °C. The $SrTiO_3$ (i.e., A region) and $SrBi_4Ti_4O_{15}$ (i.e., B region) phases are confirmed by EDS analysis (Table 1) and electron diffraction. Besides, the EDS results show that the amounts of Bi^{3+} detected in regions C (6.06 at %) and D (8.94 at %) are much less than that in region B (16.20 at %), and Sr:Ti atomic ratios in regions C (0.89:1) and D (0.87:1) are much higher than that in region B (0.25:1), implying that $(Bi_2O_2)^{2+}$ slabs began to decompound from the $SrBi_4Ti_4O_{15}$ crystal lattice and Sr^{2+} started to diffuse into pseudo-perovskite blocks to replace Bi^{3+} ions in the A-site. However, the compositions of the poorly crystalline intermediate phase(s) in reacting zones could not be estimated by EDS analysis because of possible intermixing of several intermediate phases with nanocrystalline $SrTiO_3$. Some pores and defects generally parallel to the microcrystal surface are also presented inside the platelet, especially near the interface between the reacting zone and the $SrBi_4Ti_4O_{15}$ zone (Figure 7c) or reacting zones (Figure 7d). Exfoliation of the platelet microcrystal is observed to occur at 775 °C (Figure 7a), most likely due to the expulsion of Bi_2O_3 based phases formed as a byproduct of the conversion process and loss of epitaxy during this process.

Table 1. Atomic Compositions Calculated from EDS Data for A, B, C, and D Regions Marked in Figure 7b[a]

region	Sr (at %)	Bi (at %)	Ti (at %)	Sr/Bi/Ti ratio
A	18.23 ± 1.40	1.26 ± 0.60	18.61 ± 0.76	3.92:0.27:4
B	4.06 ± 0.71	16.20 ± 0.92	16.44 ± 0.08	0.99:3.94:4
C	14.88 ± 0.68	6.06 ± 0.74	16.82 ± 0.59	3.54:1.44:4
D	13.67 ± 0.93	8.94 ± 0.53	15.81 ± 1.54	3.46:2.26:4

[a] Each data point represents the mean value of six different positions in each region.

On the basis of the above results, the overall topochemical conversion from Aurivillius $SrBi_4Ti_4O_{15}$ platelike precursors to perovskite $SrTiO_3$ microplatelets is proposed to mainly experience two stages: (i) topochemical reactions and (ii) recrystallization and grain growth. During the first stage, three types of reactions may mainly happen: (a) Sr^{2+} ions from the reactants diffuse to the (001) oriented surfaces and lateral faces of each Aurivillius $SrBi_4Ti_4O_{15}$ platelet, replace Bi^{3+}, and react with Ti^{4+} and O^{2-}, to form $SrTiO_3$ zones. The multiple topotactic nucleation events of perovskite $SrTiO_3$ directly occur on the $SrBi_4Ti_4O_{15}$ precursor surfaces and lateral faces. (b) $(Bi_2O_2)^{2+}$ sublayers react with ambient O and decompound from the $SrBi_4Ti_4O_{15}$ crystal lattice in the form of Bi_2O_3 based liquid phases. (c) Sr^{2+} ions from the reactants penetrate into the interior of each $SrBi_4Ti_4O_{15}$ platelet and diffuse into the $SrBi_4Ti_4O_{15}$ crystal lattice, and replace Bi^{3+} in the pseudo-perovskite $(SrBi_2Ti_4O_{13})^{2-}$ blocks, forming intermediate layer structured phase(s). Subsequently, the $SrTiO_3$ perovskite phase forms from related intermediate phase(s) inside $SrBi_4Ti_4O_{15}$ platelets. During the topochemical reaction, exfoliation of the partially converted microcrystal occurs, possibly due to the expulsion of Bi_2O_3 based boundary phases and loss of epitaxy. After topochemical reaction, each original (001) oriented $SrBi_4Ti_4O_{15}$ single crystal is replaced by (001) aligned perovskite-phase $SrTiO_3$ crystallites. During the second stage, these aligned perovskite aggregates recrystallize and sinter to form dense $SrTiO_3$ platelets. Most (001) oriented $SrTiO_3$ perovskite particles fabricated by the topochemical conversion are polycrystalline in nature, as evidenced by grain boundaries observed in those microplatelets.

4. CONCLUSIONS

The mechanism of topochemical microcrystal conversion was investigated during the synthesis of (001) oriented perovskite

$SrTiO_3$ microplatelets from Aurivillius $SrBi_4Ti_4O_{15}$ precursors with the same orientation. We found that the distinct $SrTiO_3$ nanocrystallite phase began to form by nucleation and growth on the (001) surfaces and lateral faces of $SrBi_4Ti_4O_{15}$ platelets heated at 750 °C. Both raw $SrBi_4Ti_4O_{15}$ zones and reacting zones containing intermediate phase(s) with less Bi^{3+} contents coexisted inside the platelet heated at 775 °C, implying that $(Bi_2O_2)^{2+}$ sublayers began to decompound from the $SrBi_4Ti_4O_{15}$ crystal lattice and Sr^{2+} started to diffuse into the pseudo-perovskite block to replace Bi^{3+} ions in the A-site. Exfoliation of the platelet microcrystals was observed to occur, possibly caused by the expulsion of byproduct Bi_2O_3 at phase boundaries and the loss of epitaxy. The $SrBi_4Ti_4O_{15}$ phase was consumed and completely converted into perovskite $SrTiO_3$ and intermediate phases at 950 °C. Further increasing the temperature and/or holding time allowed for further formation of the $SrTiO_3$ perovskite phase from related intermediate phase(s) and subsequential recrystallization and grain growth of the aligned crystallites into (001) oriented $SrTiO_3$ microplatelets. The obtained $SrTiO_3$ microplatelets preserved the shape of $SrBi_4Ti_4O_{15}$ precursors and had an average length of about 5 μm and an average thickness of around 0.4 μm. These high-aspect-ratio $SrTiO_3$ microplatelets should have general applicability for templating the grain growth of textured ceramics and seeding polycrystal conversion into single crystals to maximize electrical properties for practical applications. We believe that the investigation of the formation mechanism of $SrTiO_3$ would be very useful to guide the design and synthesis of novel anisotropic perovskite crystals with high quality in general.

■ AUTHOR INFORMATION

Corresponding Authors

*Tel(Fax): +86-451-86402771. E-mail: changyunfei@hit.edu.cn (Y.C.).
*E-mail: binyang@hit.edu.cn (B.Y.).

Notes

The authors declare no competing financial interest.

■ ACKNOWLEDGMENTS

This work was supported by the National Key Basic Research Program of China (973 Program) under Grant No. 2013CB632900, the National Science and Technology Support Program (Grant No. SQ2012BAJY3766), the Fundamental Research Funds for the Central Universities and Program for Innovation Research of Science in Harbin Institute of Technology (Grant No. 01508451), and the State Key Laboratory of New Ceramic and Fine Processing Tsinghua University.

■ REFERENCES

(1) Messing, G. L.; Trolier-McKinstry, S.; Sabolsky, E. M.; Duran, C.; Kwon, S.; Brahmaroutu, B.; Park, P.; Yilmaz, H.; Rehrig, P. W.; Eitel, K. B.; Suvaci, E.; Seabaugh, M.; Oh, K. S. *Crit. Rev. Solid State Mater. Sci.* **2004**, *29*, 45–96.

(2) Chang, Y. F.; Poterala, S.; Yang, Z. P.; Trolier-McKinstry, S.; Messing, G. L. *Appl. Phys. Lett.* **2009**, *95*, 232905.

(3) Maurya, D.; Zhou, Y.; Yan, Y. K.; Priya, S. *J. Mater. Chem. C* **2013**, *1*, 2012–2111.

(4) Sanjaya Ranmohotti, K. G.; Josepha, E.; Choi, J.; Zhang, J.; Wiley, J. B. *Adv. Mater.* **2011**, *23*, 442–460.

(5) Li, L. H.; Deng, J. X.; Yu, R. B.; Chen, J.; Wang, X. W.; Xing, X. R. *Inorg. Chem.* **2010**, *49*, 1397–1403.

(6) Montasserasadi, D.; Mohanty, D.; Huq, A.; Heroux, L.; Payzant, E. A.; Wiley, J. B. *Inorg. Chem.* **2014**, *53*, 1773–1778.

(7) Madaro, F.; Tolchard, J. R.; Yu, Y. D.; Einarsrud, M. A.; Grande, T. *CrystEngComm* **2011**, *13*, 1350–1359.

(8) Xu, S.; Li, J. F. *J. Am. Ceram. Soc.* **2011**, *94*, 3812–3818.

(9) Poterala, S.; Chang, Y. F.; Clark, T.; Meyer, R. J.; Messing, G. L. *Chem. Mater.* **2010**, *22*, 2061–2068.

(10) Wu, M. J.; Li, Y. X. *Mater. Lett.* **2010**, *64*, 1157–1159.

(11) Yan, X. B.; Gao, F.; Liu, Z. T. *Mater. Lett.* **2013**, *109*, 313–315.

(12) Rowley, S. E.; Spalek, L. J.; Smith, R. P.; Dean, M. P. M.; Itoh, M.; Scott, J. F.; Lonzarich, G. G.; Saxena, S. S. *Nat. Phys.* **2014**, *10*, 367–372.

(13) Irie, H.; Maruyama, Y.; Hashimoto, K. *J. Phys. Chem. C* **2007**, *111*, 1847–1852.

(14) Haeni, J. H.; Irvin, P.; Chang, W.; Uecker, R.; Reiche, P.; Li, Y. L.; Choudhury, S.; Tian, W.; Hawley, M. E.; Craigo, B.; Tagantsev, A. K.; Pan, X. Q.; Streiffer, S. K.; Chen, L. Q.; Kirchoefer, S. W.; Levy, J.; Schlom, D. G. *Nature* **2004**, *430*, 758–760.

(15) Ohta, H.; Sugiura, K.; Koumoto, K. *Inorg. Chem.* **2008**, *47*, 8429–8436.

(16) Sun, P. H.; Nakamura, T.; Shan, Y. J.; Inaguma, Y.; Itoh, M.; Kitamura, T. *Jpn. J. Appl. Phys.* **1998**, *37*, 5625–5629.

(17) Kalyani, V.; Vasile, B. S.; Ianculescu, A.; Buscaglia, M. T.; Buscaglia, V.; Nanni, P. *Cryst. Growth Des.* **2012**, *12*, 4450–4456.

(18) Lehuta, K. A.; Kittilstved, K. R. *J. Mater. Chem. A* **2014**, *2*, 6138–6145.

(19) Rabuffetti, F. A.; Kim, H. S.; Enterkin, J. A.; Wang, Y. M.; Lanier, C. H.; Marks, L. D.; Poeppelmeier, K. R.; Stair, P. C. *Chem. Mater.* **2008**, *20*, 5628–5635.

(20) Hu, L.; Wang, C.; Lee, S.; Winans, R. E.; Marks, L. D.; Poeppelmeier, K. R. *Chem. Mater.* **2013**, *25*, 378–384.

(21) Watari, K.; Brahmaroutu, B.; Messing, G. L.; Trolier-McKinstry, S.; Cheng, S. C. *J. Mater. Res.* **2000**, *15*, 846–849.

(22) Liu, H.; Sun, X.; Zhao, Q.; Xiao, J.; Ouyang, S. *Solid-State Electron.* **2003**, *47*, 2295–2298.

(23) Ebrahimi, M. E.; Allahverdi, M.; Safari, A. *J. Am. Ceram. Soc.* **2005**, *88*, 2129–2132.

(24) Akdogan, E. K.; Brennan, R. E.; Allahverdi, M.; Safari, A. *J. Electroceram.* **2006**, *16*, 159–165.

(25) Liu, Y. F.; Lu, Y. N.; Xu, M.; Zhou, L. F.; Shi, S. Z. *Mater. Chem. Phys.* **2009**, *114*, 37–42.

(26) Saito, Y.; Takao, H. *Jpn. J. Appl. Phys.* **2006**, *45*, 7377–7381.

(27) Chang, Y. F.; Poterala, S.; Yener, D.; Messing, G. L. *J. Am. Ceram. Soc.* **2013**, *96*, 1390–1397.

(28) Xue, H.; Xiong, Z. X. *J. Alloys Compd.* **2009**, *467*, 338–341.

(29) Bai, W. F.; Hao, J. G.; Fu, F.; Li, W.; Shen, B.; Zhai, J. W. *Mater. Lett.* **2013**, *97*, 137–140.

(30) Lee, D. S.; Jeong, S. J.; Kim, M. S. *Jpn. J. Appl. Phys.* **2010**, *49*, 091101.

(31) Shoji, T.; Fuse, K.; Kimura, T. *J. Am. Ceram. Soc.* **2009**, *92*, S140–S145.

(32) Li, X.; Liu, P.; Xi, Z.; Fang, P.; Long, W.; Zhao, X. *J. Electroceram.* **2014**, *32*, 86–91.

(33) Nath, A. K.; Medhi, N. *Mater. Lett.* **2012**, *73*, 75–77.

(34) Su, S.; Zuo, R. Z.; Lv, D. Y. *J. Alloys Compd.* **2012**, *519*, 25–28.

(35) Su, S.; Zuo, R. Z.; Lv, D. Y.; Fu, J. *Powder Technol.* **2012**, *217*, 11–15.

(36) Chang, Y. F.; Wu, J.; Yang, B.; Zhang, S. T.; Lv, T. Q.; Cao, W. W. *Mater. Lett.* **2014**, *129*, 126–129.

(37) Chang, Y. F.; Lee, S. N.; Poterala, S.; Randall, C. A.; Messing, G. L. *J. Mater. Res.* **2011**, *26*, 3044–3050.

(38) Guo, C. L.; Wu, Y. Q. *Acta Phys. Sin.* **1980**, *29*, 1491.

(39) Megaw, H. D. *Proc. Phys. Soc., London* **1946**, *58*, 133.

(40) Kojima, S.; Imaizumi, R.; Hamazaki, S.; Takashige, M. *Jpn. J. Appl. Phys.* **1994**, *33*, 5559–5564.

(41) Zhu, J.; Chen, X. B.; Zhang, Z. P.; Shen, J. C. *Acta Mater.* **2005**, *53*, 3155–3162.

(42) Nilsen, W. G.; Skinner, J. G. *J. Chem. Phys.* **1968**, *48*, 2240–2248.

(43) Petzelt, J.; Ostapchuk, T.; Gregora, I.; Rychetsky, I.; Hoffmann-Eifert, S.; Pronin A, V.; Yuzyuk, Y.; Gorshunov, B. P.; Kamba, S.; Bovtun, V.; Pokorny, J.; Savinov, M.; Porokhonskyy, V.; Rafaja, D.; Vanek, P.; Almeida, A.; Chaves, M. R.; Volkov, A. A.; Dressel, M.; Waser, R. *Phys. Rev. B* **2001**, *64*, 184111.